Dynamical phase transitions in one-dimensional hard-particle systems

Ian R. Thompson and Robert L. Jack
Department of Physics, University of Bath, Bath BA2 7AY, United Kingdom
(Received 5 June 2015; revised manuscript received 28 August 2015; published 12 November 2015)

We analyze a one-dimensional model of hard particles, within ensembles of trajectories that are conditioned (or biased) to atypical values of the time-averaged dynamical activity. We analyze two phenomena that are associated with these large deviations of the activity: phase separation (at low activity) and the formation of hyperuniform states (at high activity). We consider a version of the model which operates at constant volume, and a version at constant pressure. In these nonequilibrium systems, differences arise between the two ensembles, because of the extra freedom available to the constant-pressure system, which can change its total density. We discuss the relationships between different ensembles, mechanical equilibrium, and the probability cost of rare density fluctuations.

DOI: 10.1103/PhysRevE.92.052115 PACS number(s): 05.40.−a

I. INTRODUCTION

Out-of-equilibrium systems differ from their equilibrium counterparts in many ways. For example, long-ranged correlations are generic in nonequilibrium steady states [1,2]; unusual phase transitions can take place [3]; and there may be significant differences in behavior for the same system in different ensembles (for example, canonical and grand canonical [4,5]). Recently, there has been considerable interest in large-deviation phenomena [6], based on ensembles of trajectories that are conditioned on atypical values of time-averaged observables [7–12]. In glassy systems, ensembles conditioned on the dynamical activity quite generically support phase transitions between active and inactive states [9,13]. In other systems, such biases can result in phase separation [14], and other kinds of phase transition [7].

Here, we consider large deviations of the activity in a model of hard particles that diffuse in one dimension. Considering this system in a constant-volume ensemble, we showed previously [15] that a bias to lower than average activity leads to phase-separated states, in which the density becomes macroscopically inhomogeneous. Also, on biasing to higher than average activity, we found that the system enters a hyperuniform state, in which large-scale density fluctuations are strongly suppressed [16]. On large length and time scales, the system can be described by fluctuating hydrodynamics and the macroscopic fluctuation theory [17,18], and both phase separation [14] and hyperuniformity [15] can be predicted from these theories.

In this work, we extend these results in three ways. First, we analyze the phase-separated state in more detail, including a finite-size scaling analysis, an analysis of the balance of forces at the interface between the dense and dilute phases, and the stability of the phase-separated state. Second, we consider the same hard-particle system in a constant-pressure ensemble. That is, we allow the system size to fluctuate, coupling it to a barostat that enforces a given mechanical pressure. For the system at equilibrium, the implementation of the barostat is standard [19], and is chosen so that the constant-pressure system resembles a typical subsystem of a very large constant-volume system. However, on biasing the system to nontypical dynamical activity, the constant-pressure system no longer mirrors the behavior of a subsystem of the constant-volume one: for a bias to low activity, the constant-volume system exhibits phase coexistence between dense and dilute phases, but the constant-pressure one has only a dense phase. For high activity, hyperuniformity is less apparent in the constant-pressure system, which tends instead to reduce its total density. We discuss how equivalence between constant-pressure and constant-volume ensembles should be interpreted in systems exhibiting large deviations.

Third, we analyze the mechanical pressure within these systems, as a function of the bias to low (or high) activity. The pressure is defined by analogy with the virial pressure in equilibrium systems, by considering the force exerted on one region of the system by other neighboring regions. In the phase-separated state, this pressure is not constant throughout the system, in stark contrast to the situation in equilibrium systems at phase coexistence. Describing the system in terms of a Langevin equation, we show how pressure gradients are balanced by noise forces that acquire finite average values, due to the low-activity bias on the system. Similar phase coexistence phenemona appear in active matter systems: we argue that particles' swimming forces in those systems act similarly to biased noises, and can balance pressure gradients [20–23].

Taken together, our results highlight the broad range of phenomena that can occur in conditioned (or biased) ensembles of trajectories, even in simple models. They show that equilibrium ideas of pressure and ensemble equivalence can sometimes be applied in these contexts, but that these applications may be subtle and require careful justification. In the following, Sec. II describes the models and methods that we will use, Sec. III shows results for constant-volume systems, while Sec. IV includes results at constant pressure. In Sec. V, we discuss force balance and mechanical equilibrium in these systems. We draw our conclusions in Sec. VI.

II. MODEL AND METHODS

A. Model

1. Constant volume

We consider N hard particles undergoing Brownian motion in one dimension, with periodic boundaries. Particle motion is

described by the overdamped Langevin equation:

$$\dot{x_i} = -\frac{D_p}{k_B T}\nabla_i U + \sqrt{2D_p}\eta_i(t), \tag{1}$$

where x_i is the position of particle i, U is the potential energy of the system, D_p is the diffusion coefficient for particle motion, and $\nabla_i = (\partial/\partial x_i)$. The notation $\dot{x} \equiv (\partial x/\partial t)$ and we use Ito's convention for stochastic differential equations throughout [24]. The random noise η_i has zero mean and is uncorrelated in time and space:

$$\langle \eta_i(t)\eta_j(t')\rangle = \delta(t-t')\delta_{ij}. \tag{2}$$

One may easily show [24] that the steady state of this system is a Boltzmann distribution $p(x) \propto \exp[-U(x)/k_B T]$.

We consider the case where the energy U is given by a pair potential, $U = \frac{1}{2}\sum_{i\neq j} v(x_i - x_j)$. Specifically, we consider hard particles of size l_0,

$$v(x) = \begin{cases} \infty, & \text{if } |x| \leqslant l_0, \\ 0, & \text{otherwise.} \end{cases} \tag{3}$$

In this case, particles cannot interpenetrate or otherwise move past one another, leading to single-file diffusion [25]. [For the derivatives in (1) to make sense, one should regularize the potential by smoothing its discontinuities, so that the hard-particle case may be obtained by taking a suitable limit. In practice, we use a Monte Carlo scheme to solve the equation, which avoids the requirement for any explicit regularization.]

In one dimension, the equation of state for this system is simply that of an ideal gas with excluded volume:

$$P(L - Nl_0) = Nk_B T, \tag{4}$$

where P is the pressure. We also define the packing fraction $\phi = \frac{Nl_0}{L}$. Finally, the natural time scale in the system is the *Brownian time*, which is the time taken for the root mean squared displacement of a free particle to reach its own length,

$$\tau_B = \frac{l_0^2}{2D_p}. \tag{5}$$

2. *Constant pressure*

To define a constant pressure version of the model, we allow the total system size L to fluctuate, so the state of the system is specified by the positions of its N particles, $(x_1, x_2, \ldots, x_N)$, and the total system size L. It is useful to define rescaled coordinates $u_i = x_i/L$. The particle positions evolve according to (1) as before, and the appropriate equation of motion for the system size is

$$\dot{L} = -\frac{D_L}{k_B T}(P - \mathcal{P}_{\rm vir}) + \sqrt{2D_L}\eta_L(t), \tag{6}$$

where the parameters P and D_L are the applied pressure and a diffusion constant for the system size variable L, while the (instantaneous) virial pressure of the system depends on the particle coordinates as $\mathcal{P}_{\rm vir} = (Nk_B T/L) + \frac{1}{2L}\sum_i (x_i - x_{i+1})v'(x_{i+1} - x_i)$ [19], where $v'(x) = (d/dx)v(x)$ is the derivative of the interaction potential. [As discussed above, some regularization of $v(x)$ is required but this will be unimportant in the following.] The noise term η_L has zero mean, with $\langle \eta_L(t)\eta_L(t')\rangle = \delta(t-t')$, and $\eta_L(t)$ is independent of the other noises $\eta_i(t)$.

The equation of motion (6) may be justified in several ways. Constructing the appropriate Fokker-Planck equation for this system [24], one finds that the steady state probability distribution for the particle coordinates and size of this system is the appropriate Boltzmann distribution $p(x, L) \propto L^N \exp[-(PL + U)/k_B T]$, where U is the potential energy, as above. The steady state of the system is also time-reversal symmetric, as required for an equilibrium state. For an alternative motivation, one might define the system in terms of its MC dynamics, which are the standard ones for constant-pressure systems (see Sec. II A 3 and Appendix A, below). In that case, the Langevin equations (1,6) may be derived from the Monte Carlo (MC) scheme, in the limit of small time step [26]. In either case, the important feature is that these equations describe a diffusive dynamics whose steady states are the appropriate constant-volume or constant-pressure equilibrium states of hard particles in one dimension.

So far, the diffusion constant D_L is a free parameter, since the model converges to the correct equilibrium distribution, whatever the value of D_L. However, as anticipated in the Introduction, the dynamical properties of our constant pressure system (at equilibrium) are chosen to mimic those of a subsystem of the constant-volume one. This requires a suitable choice for D_L, as we now explain by a hydrodynamic argument, based on the behavior of large systems.

If we take an equilibrium average of (6) and work in the steady state, $\langle \dot{L}\rangle = 0$, we find

$$P = \langle \mathcal{P}_{\rm vir}\rangle, \tag{7}$$

confirming that the steady state of the system has an (average) virial pressure equal to P, as required. For large systems, the system size is almost always close to its mean value $\overline{L} = \langle L\rangle$, with small fluctuations of size $O(\sqrt{N})$. Further, if the system size L fluctuates to a value $\overline{L} + \delta L$ that is slightly larger than its average value then the virial pressure of the system will be $\mathcal{P}_{\rm vir} \approx P - \delta L/(\overline{L}\kappa_T)$, where $\kappa_T = (-1/\overline{L})(\partial L/\partial P)$ is the isothermal compressibility. Inserting this relation into (6) and taking the average over the stochastic dynamics, one arrives at a deterministic equation for the relaxation of this system-size fluctuation $\dot{\delta L} = -\frac{D_L}{k_B T}\frac{1}{\overline{L}\kappa_T}\delta L$. Solving this equation, one sees that fluctuations in the system size L relax on a time scale $\tau_{LL} = (\overline{L}\kappa_T k_B T/D_L)$.

To fix the value of D_L, we note that for a large constant-volume system, density fluctuations on a length scale R should relax on a time scale of order $\tau_\rho(R) = R^2/[(2\pi)^2 D_c]$, where D_c is a collective diffusion constant. We assume that D_c is similar to the bare particle diffusion constant D_p (this assumption can be justified within a fluctuating hydrodynamic or macroscopic fluctuation theory approach [17,27]). We then match time scales between constant-volume and constant pressure systems by setting $\tau_{LL} = \tau_\rho(\overline{L})$, which yields

$$D_L \simeq (2\pi)^2 \frac{D_p \kappa_T k_B T}{\overline{L}}. \tag{8}$$

The numerical prefactor in this equation is not crucial for this work but the scaling of D_L with system size $\overline{L}$ will be important in what follows.

3. Monte Carlo dynamics

In our numerical simulations of this model, we use a Monte Carlo dynamical scheme. Details are given in Appendix A. The scheme includes a time step t_0 as an explicit parameter, and the maximal displacement of a particle in a single MC move is $S = \sqrt{6 D_p t_0}$. In the limit of small t_0, the MC method is equivalent to solving the Langevin equations (1) and (6).

B. Large deviations

As anticipated in the Introduction, we will be concerned here with ensembles of trajectories which are biased to nontypical values of an "activity" parameter K. The methodology that we use is now well established (see for example [7,9,10,13]): our specific approach is described in this section and follows closely that of [9]. A trajectory of the system is a realization of the system developing through time. A trajectory has a time duration $t_{\rm obs}$ which is composed of M smaller and consecutive "slices" of time, each of length Δt, such that $t_{\rm obs} = M \Delta t$.

To define the activity K, we measure the squared displacements of all particles during each slice and sum over the M slices in a trajectory:

$$K[x(t)] = \sum_{j=1}^{M} \sum_{i=1}^{N} |x_i(j\Delta t) - x_i((j-1)\Delta t) - \Delta \overline{x}_j|^2, \quad (9)$$

where the notation $[x(t)]$ indicates a functional dependence on all particle positions throughout a trajectory. The quantity $\Delta \overline{x}_j = (1/N) \sum_i \{x_i(j\Delta t) - x_i[(j-1)\Delta t]\}$ is the change of the center of mass position during the jth slice: for large systems this term has a negligible effect on K but subtracting it in this way helps to minimize finite-size effects in simulations. It is often useful to normalize the activity as

$$k = \frac{K}{L t_{\rm obs}}. \quad (10)$$

(For the constant pressure systems, we replace L by $\overline{L}$ in this equation.) We take the time interval $\Delta t = \tau_B$, so that K depends on movement of particles on length scales comparable with their size, consistent with [9]. Figure 1 shows the dependence of the activity k on the packing fraction ϕ and the MC step size S.

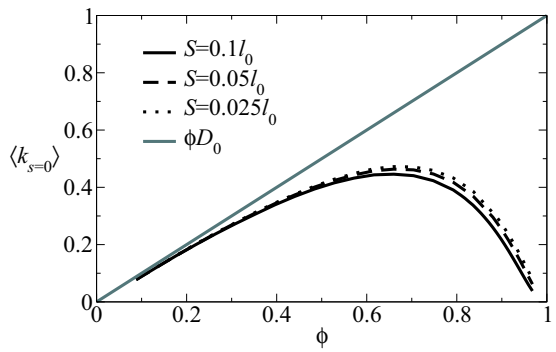

FIG. 1. (Color online) Equilibrium activity k as a function of the packing fraction ϕ and the maximum MC step S in the constant-volume ensemble. The activity is linear in ϕ for small packing fractions, because k is proportional to the number of particles per unit volume. For larger ϕ, particles start to obstruct each other and the activity falls.

The large deviation formalism uses a biasing field s to investigate trajectories where $t_{\rm obs}$ is large but the activity k deviates significantly from its typical value. To this end, we define a probability distribution over the trajectories of the system:

$$P_s[x(t)] = \frac{P_0[x(t)] e^{-sK[x(t)]}}{Z(s, t_{\rm obs})}, \quad (11)$$

where $Z(s,t_{\rm obs}) = \langle e^{-sK} \rangle_{\rm eq}$ is a dynamical partition function (the average is evaluated at equilibrium). By analogy with equilibrium thermodynamics, we interpret $\psi(s,t_{\rm obs}) = -(L t_{\rm obs})^{-1} \ln Z(s,t_{\rm obs})$ as a dynamical free energy (or free energy density). For large L and $t_{\rm obs}$, the free energy may develop a singular dependence on s, which signals the presence of phase transitions.

We use a notation $\langle \cdot \rangle_s$ to indicate averages with respect to the distribution (11). The free energy $\psi(s)$ is a scaled cumulant generating function, so it is easily verified that the mean activity $k(s,t_{\rm obs}) \equiv (L t_{\rm obs})^{-1} \langle K \rangle_s$ is obtained by taking a derivative: $k(s) = (\partial \psi / \partial s)$, while the susceptibility $\chi(s,t_{\rm obs}) \equiv (L t_{\rm obs})^{-1} \langle (K - \langle K \rangle_s)^2 \rangle_s$ is equal to $-(\partial k / \partial s)$. For large $t_{\rm obs}$, taking averages with respect to the distribution (11) is equivalent to studying trajectories of that system that are conditioned to (nontypical) values of the activity k [11,12]. The equivalence is similar to that between microcanonical and canonical ensembles in equilibrium statistical mechanics, and means that the main results shown here could also be obtained by considering trajectories conditioned on K. The approach using the bias s is more convenient both computationally and analytically; see for example [2,7–9].

C. Transition path sampling

To sample the biased ensemble of trajectories given in (11), we use transition path sampling [28,29], following the implementation of [9,10]. An initial trajectory is generated from an equilibrium initial configuration by simulating the dynamics of a system for a duration $t_{\rm obs}$. A new trajectory is created by copying a randomly selected portion of the first trajectory to either the start or end of the new trajectory. The rest of the new trajectory is then generated according to the relevant Langevin equations. The new trajectory is compared to the first and replaces it with probability

$$P_{\rm accept} = \min\{1, e^{-s\Delta K}\}, \quad (12)$$

where $\Delta K = K_{\rm new} - K_{\rm old}$. Generation then continues using the most recently accepted trajectory as the parent. Using this method means that, after many iterations, the algorithm samples trajectories according to the distribution defined in (11).

III. RESULTS: CONSTANT-VOLUME SYSTEM

In this section we present results for biased ensembles of the hard-particle system in the NVT (constant volume) ensemble. All results are for the case $\phi = 0.88$, as in [15], which is a relatively high density: it gives a mean free space per particle of $0.136 l_0$ and a typical time between collisions of $0.018 \tau_{\rm B}$.

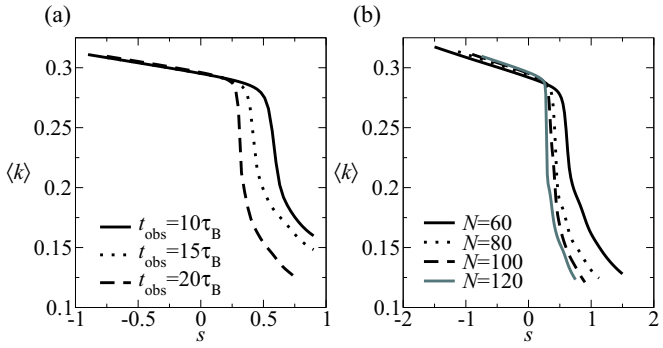

FIG. 2. (Color online) The average activity k for constant-volume systems at $\phi = 0.88$. (a) Behavior of the activity for a system of $N = 100$ particles, varying t_{obs}. (b) The effect of changing the number of particles in the system at constant $t_{obs} = 20\tau_B$.

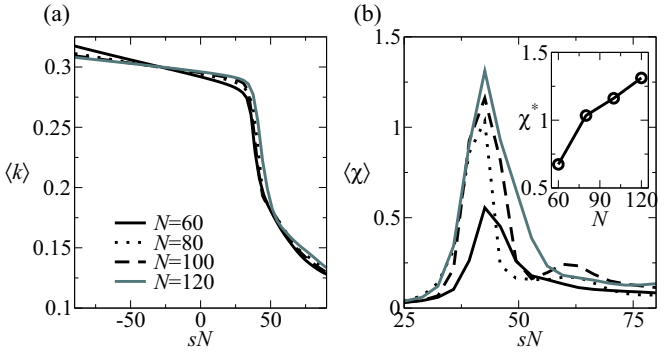

FIG. 3. (Color online) Scaling of the transition with system size. (a) The activity $k(s)$ collapses onto a single curve as a function of sN. (b) Similarly, the peak in the dynamic susceptibility occurs at $s^* \sim N$. Inset: The maximal susceptibility χ^* increases with increasing system size, showing that the magnitude of the activity fluctuations is increasing.

This is a diffusive system and is described by the theory of fluctuating hydrodynamics (or macroscopic fluctuation theory) [17,18]. Based on this theory, we expect qualitative aspects of the system's behavior to be independent of ϕ [15].

A. Phase separation for $s > 0$

We first consider the effect of a bias $s > 0$, which leads to a phase transition in this system [15]. Phase transitions are signalled by singularities in the free energy $\psi(s)$, which appear only in the limit when both the observation time t_{obs} and the system size N are very large. Figure 2 shows the average activity $k(s)$ for different system sizes and observation times. In particular, Fig. 2(a) shows the effect of increasing t_{obs} at fixed system size $N = 100$, while Fig. 2(b) shows dependence on system size N, all obtained for large $t_{obs} = 20\tau_B$. Similar results were shown in [15]: here we analyze this behavior in more detail.

As in glass-forming systems [9,13], biasing to low dynamical activity yields a crossover at some $s = s^*$, from active to inactive dynamics. The value of s^* is positive and depends on both N and t_{obs}. The properties of the crossover can be obtained by a finite-size scaling analysis, which involves a joint limit of large system size N and large observation time t_{obs} [9,14,30,31]. In this limit, the crossover becomes a sharp discontinuity in $k(s)$. To rationalize this behavior, note that for $s \to \infty$, the system must arrive at the state with minimal propensity for activity [15], which is the fully phase-separated state, where the particles in the dense cluster are all touching each other. It is therefore clear that phase separation must occur at some field s^*. In fact, this phase transition can be predicted and analyzed in detail in the framework of fluctuating hydrodynamics [1,17,32], which predicts that the system will phase separate whenever $(\partial^2/\partial\rho^2)\langle K\rangle_{eq} < 0$, and that $s^* \sim N^{-2}$ tends to zero as the system gets large [14,15,27].

Figure 3 shows a finite-size scaling analysis of the transition. For fixed $t_{obs} = 20\tau_B$ and increasing N, we find $s^* \sim N^{-1}$, as indicated by the collapse of $k(s)$ and the scaling of the peak in the susceptibility χ. It seems that the theoretical prediction that $s^* \sim N^{-2}$ [14,27] may be observable only for larger-N and/or larger t_{obs}: we discuss this possibility in Sec. III C.

B. Structure of the phase-separated state

Figure 4 shows trajectories from biased ensembles, both at equilibrium and for an inactive state. At $s = 0$ the system is an equilibrium fluid of hard particles. In the inactive phase [$s > s^*$, Fig. 4(b)] the system phase separates throughout the whole trajectory: one observes a significant region that is devoid of particles, with the remainder of the system increasing its local density to incorporate the empty region. At the beginning and end of the trajectory, the empty region shrinks slightly: this behavior is also expected, since biases on dynamical activity have their strongest effects in the bulk of the trajectory, with slightly weaker influence near the initial and final times [30].

To probe the structure of these systems it is convenient to make a change of coordinates. The system is one dimensional and the particles are hard, so the ordering of the particle coordinates is fixed: there is no "overtaking." We number particles so that their coordinates are in an increasing sequence, and define new coordinates $X_j = x_j - jl_0$ which are also ordered

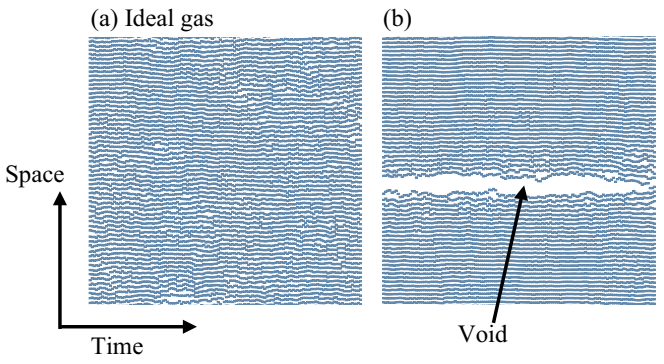

FIG. 4. (Color online) Trajectories of a constant-density system at $N = 60$, $\phi = 0.88$, and $t_{obs} = 20\tau_B$. Particles are shown in blue; their diffusive time evolution leads to "world lines" that run from left to right. (a) Equilibrium state, $s = 0$, in which the particles form a (diffusive) ideal gas. (b) Effect of a bias to low activity, $s = 1.25$. The system phase separates into a large dense cluster and an empty "void" space.

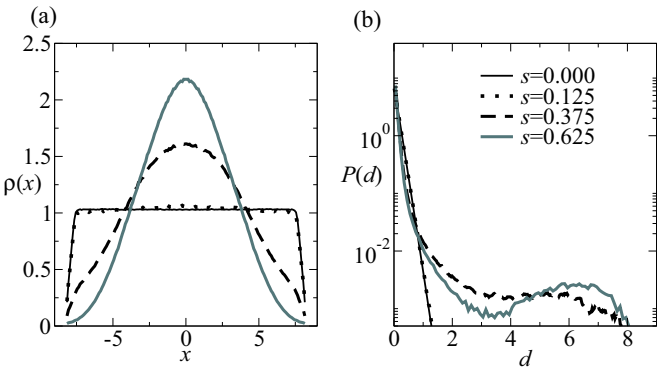

FIG. 5. (Color online) Structural measurements in the constant-volume system with point particles at $\frac{N}{L'} = 7.33/\ell_0$ with $N = 120$, for equilibrium and inactive systems. (a) Measurements of the one-body density $\rho(x)$ for homogeneous and phase-separated states. (b) Distribution of separations for the equilibrium and inactive phases.

in the same way. The X_j are coordinates of point particles in a system of size $L' = L - Nl_0$. At equilibrium, the positions X_j are uncorrelated—they represent positions of ideal gas particles. For example, if we define a Fourier-transformed density $\delta\rho_q = \sum_j e^{-iqX_j}$ and calculate the structure factor

$$S(q) = \frac{1}{L'}\langle \delta\rho_q \delta\rho_{-q}\rangle \tag{13}$$

then we find $S(q) = N/L' = \frac{\phi}{l_0(1-\phi)}$, independent of q.

Now define d_i as the separation between particle i and its right neighbor,

$$d_i = x_{i+1} - x_i. \tag{14}$$

In order to investigate the one-body density profile associated with the phase-separated state illustrated in Fig. 4(b), it is necessary to fix an origin. We accomplish this by finding the largest "gap" d_i in any configuration. We choose a random point within that gap, and we place the origin the maximal possible distance, $L'/2$, from that point. Thus the origin almost certainly lies within the dense phase. The density of point particles is then $\rho(X) = \sum_j \delta(X - X_j)$, where X_j is now measured with respect to this new origin. We average $\rho(X)$ to obtain the one-body densities shown in Fig. 5(a). At equilibrium, the density profile is uniform, as expected (up to weak boundary effects that arise because the origin was constrained to lie far from the largest gap).

The distribution of separations, $P(d)$, was also recorded for systems at $s = 0$ and $s > s^*$. This is shown in Fig. 5(b). At equilibrium, one finds an exponential distribution, typical of a $1d$ equilibrium fluid. However, the distribution of separations in the inactive phase is bimodal. For small d, the distribution is approximately exponential but with a smaller characteristic length scale than the equilibrium fluid: this corresponds to particles within the dense region of the system. For larger d, there is a broad distribution of separations that comes from pairs of particles located on opposite sides of the large void (each configuration contributes only a single sample to the large-d peak, so the width of this peak appears only after averaging many configurations). These separations are comparable to the system size: together with the inhomogeneous density profiles in Fig. 5, they provide quantitative characterization of the phase separation shown in Fig. 4(b).

C. Stability of the phase-separated state

The phenomenon of phase separation is not expected in one-dimensional systems at equilibrium (assuming that forces are short ranged). We therefore explore the physics behind this effect in more detail. One can estimate the probability that the trajectory shown in Fig. 4(b) would occur at equilibrium, as follows. The particles within the large cluster are constrained by their neighbors and their contributions to the activity K are necessarily small. The particles at the boundaries of the cluster cannot move into the cluster, but they may move away from it. The probability that one of these particles nevertheless remains close to the edge of the cluster for the whole time $t_{\rm obs}$ scales as $e^{-\gamma t_{\rm obs}}$, where γ is a parameter with units of inverse time, proportional to the rate for diffusion of the particle away from the cluster.

The key point is that maintaining the integrity of the cluster requires only that the two particles at its boundaries do not move away. Hence, for large $t_{\rm obs}$, the probability $P_{\rm ps}$ of a phase-separated state at equilibrium should satisfy $\ln(P_{\rm ps}/P_{\rm eq}) \gtrsim -2\gamma t_{\rm obs}$, where $P_{\rm eq}$ is the probability of a typical equilibrium trajectory. Within the s ensemble, the ratio $(P_{\rm ps}/P_{\rm eq})$ is multiplied by a term $e^{s\Delta K}$, where ΔK is the difference in activity between equilibrium and phase-separated states. Since the activity at equilibrium is extensive (that is, $\Delta K \sim \delta k N t_{\rm obs}$), one therefore expects phase-separated states to dominate for $s \gtrsim 2\gamma/(N\delta k)$.

This argument essentially reproduces the prediction of [33] for phase transitions in kinetically constrained models; see also [13,30]. Assuming that γ is independent of N, we predict $s^* \lesssim N^{-1}$, consistent with Fig. 3. However, as discussed above, the more refined analysis available from fluctuating hydrodynamics predicts $s^* \sim N^{-2}$ [14]. That is, the bias required to stabilize phase-separated states is even less than that predicted by the simple argument given here. The reason is that the interface between high- and low-density regions of the system may not consist of a single particle, but can be smoothed out: this acts to reduce γ to a quantity of order $1/N$, further stabilizing the phase-separated state. However, it seems that the regime in which these smoothed out interfaces can be observed is not accessible within our simulations (where both N and $t_{\rm obs}$ are limited by the computational effort required).

The generalization of these arguments to higher dimensions is not immediate but we can make some tentative predictions. Let d be the spatial dimension and L the linear system size. For phase-separated states in large systems we expect the heuristic argument above to hold, with $\gamma \sim L^{d-1}$ since all particles on the boundary of a large cluster are free to diffuse away. We have $\Delta K \sim L^d$ in all dimensions so we expect a transition to a phase-separated state, with $s^* \lesssim L^{-1}$ in all dimensions. A scaling analysis within fluctuating hydrodynamics yields $s^* \sim L^{-2}$, indicating that the heuristic argument again overestimates s^*. In kinetically constrained models [13,30,34], bounds on s^* are available, based on the existence of phase-separated states where almost all particles are unable to move, due to the kinetic constraints. In this case the scaling of γ with system size depends on the specific model considered, and can lead to

very small values of s^*, as observed (for example) for the two spin facilitated triangular lattice gas model [13] for which we expect $s^* \sim L^{-d}$.

D. Hyperuniformity for $s < 0$

We now turn to the case $s < 0$, in which the system is biased to higher than average activity. In this case, the system enters a hyperuniform state [15], in which density fluctuations on large scales are strongly suppressed. In Fig. 6, we illustrate the density correlations in this state, both in real space and in reciprocal space. Panel (a) shows the pair correlation function $g(x) = \langle \rho(x')\rho(x'+x)\rangle / \langle\rho\rangle^2$ (the system is translationally invariant so there is no dependence on x'). Particles appear to repel each other, leading to a depletion zone around each particle, which facilitates motion on small length scales. However, the deviation of $g(x)$ from unity is small in absolute terms: this is a rather weak effect. Moving to Fourier space [Fig. 6(b)] reveals the strong correlations associated with hyperuniformity (similar results were shown in [15]). In contrast to the equilibrium system for which $S(q) = \text{const}$ for all q [35], one sees behavior consistent with $S(q) \to 0$ as $q \to 0$, which is the signature of hyperuniform states [16]. This transition is predicted to exist in all spatial dimensions; its scaling properties are discussed in [15]. This phenomenon has been found in jammed sphere packings [36,37] and in a range of other physical systems [15,38–40].

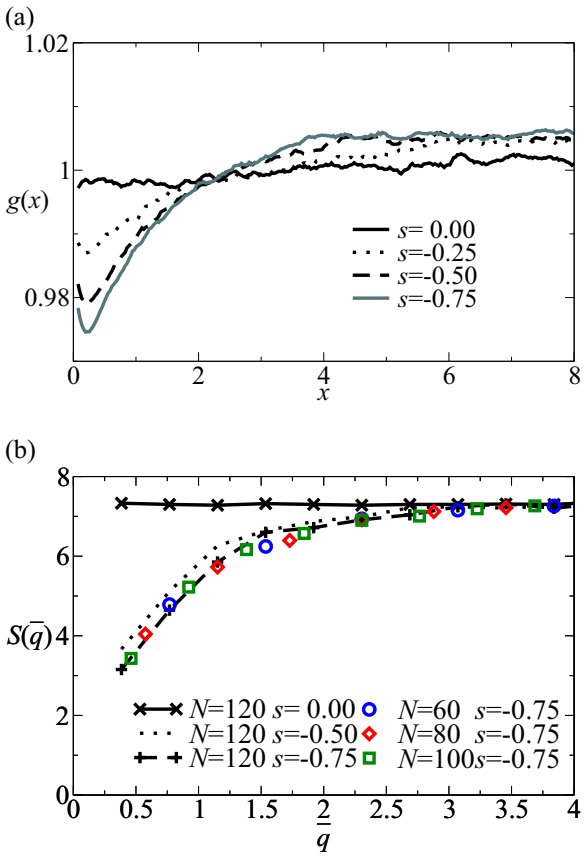

FIG. 6. (Color online) (a) The pair correlation function, $g(x)$, for point particles in the constant-density regime with $N = 120$, $t_{\text{obs}} = 20\tau_{\text{B}}$ in the active phase. The depression in $g(x)$ for small x reflects an increase in local free volume around the particles as activity increases. (b) Small q structure factor in constant-density systems. Biasing to $s < 0$ causes the suppression at small wave vectors, $S(q) \sim q$, consistent with the onset of hyperuniformity. At fixed s all system sizes collapse onto a single curve.

IV. RESULTS: CONSTANT PRESSURE

So far, we have discussed the effects of biasing the dynamical activity in the constant-volume hard-particle system, as originally discussed in [15]. We now consider the effects of a similar bias on a constant-pressure system. For consistency with the previous section, we fix the pressure at $P = 7.33(k_{\text{B}}T/l_0)$ so that the mean volume fraction at equilibrium is $\langle\phi\rangle = 0.88$.

A. Inactive state, $s > 0$

The effect of a bias to low activity, $s > 0$, is shown in Figs. 7(a) and 7(b). Comparing with Fig. 2, a similar transition is apparent, but instead of a crossover at some $s^* > 0$ that depends on N,t_{obs}, one instead observes a crossover very close to the equilibrium point $s = 0$. Note that the values of t_{obs} used here are significantly larger than those used in the constant-volume system: they are comparable with the volume

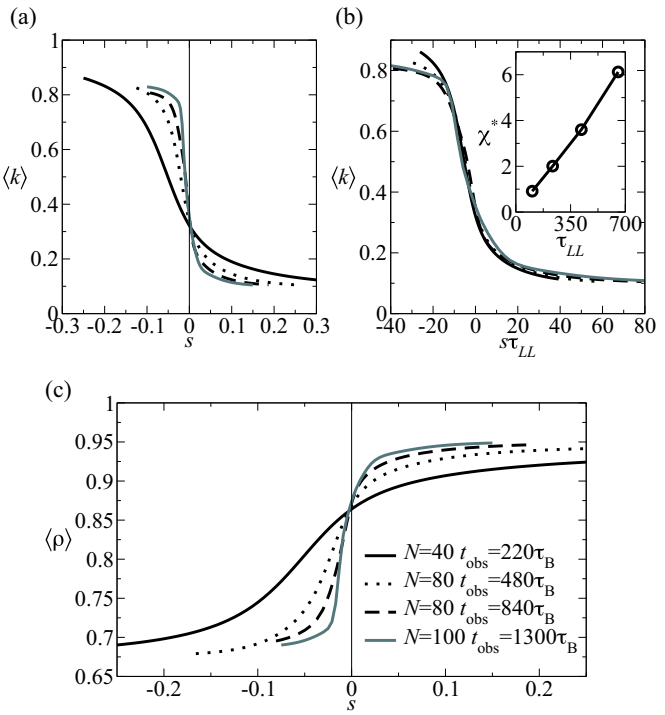

FIG. 7. (Color online) Dynamic behavior of the constant-pressure system. All results come from trajectories of duration $t_{\text{obs}} \approx 2\tau_{LL}$ at $P = 7.33(k_{\text{B}}T/l_0)$. (a) The intensive activity and dynamic susceptibility of the system as a function of s. The transition (crossover) takes place at $s^* = 0$ for all system sizes, and the width of the crossover is proportional to $(\tau_{LL})^{-1}$. (b) The data for all system sizes collapse when scaled by τ_{LL}; inset: the peak in the dynamic susceptibility scales with τ_{LL}. (c) The (total) density of the system changes as the system undergoes the transition shown in (a).

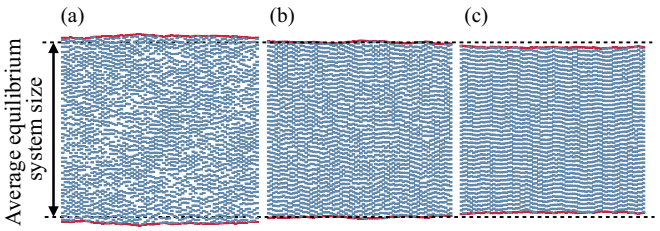

FIG. 8. (Color online) Representative trajectories of constant pressure systems at $P = 7.33(k_B T/l_0)$ with $N = 40$, $t_{obs} = 220\tau_B$ at different biases. Red lines indicate the boundaries of the system and dashed lines show the mean box size at equilibrium. (a) Active state, $s = -0.250$: the system expands, reducing its density and leading to increased activity. (b) $s = 0$, the equilibrium system has a fluctuating volume but maintains $\langle\phi\rangle = 0.88$. (c) Inactive state, $s = 0.375$: the system size is reduced relative to equilibrium, suppressing the activity.

relaxation time of the barostat $\tau_{LL} \sim \overline{L}^2$ (recall Sec. II A 2). The density of the system also shows a sharp crossover near $s = 0$; see Fig. 7(c).

Figure 8 shows representative trajectories from biased ensembles in the constant-pressure system. Comparing with Fig. 4, no phase separation occurs. We also note that the box size varies with s, consistent with Fig. 7(c).

Figure 9 shows the correlation between activity and average density for all dynamic regimes. Within the theory of fluctuating hydrodynamics [17,18], the density field is assumed to give a full description of the large-scale behavior of this system. In constant-volume systems, density fluctuations on finite wave vectors control the fluctuations in activity [15,27]. In the constant pressure system, Fig. 9 shows that the total density (i.e., the density at zero wave vector) correlates strongly with the activity: high density is associated with low activity, and vice versa.

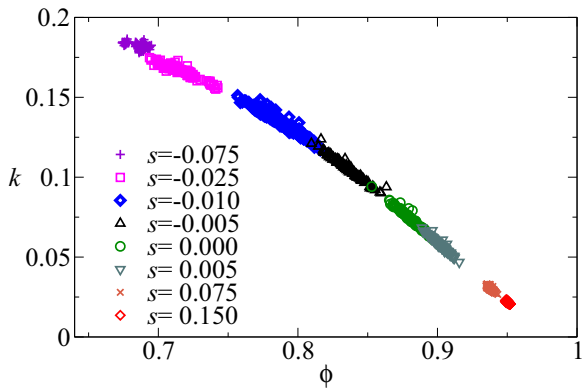

FIG. 9. (Color online) Scatter plot of activity against the average density of trajectories of duration $1300\tau_B$ with $N = 100$ particles from biased ensembles. There is a strong correlation between the activity and the density of the trajectories. The data come from ensembles with a range of bias strengths, as shown, and cover a wide range of density and activity. The gaps between data sets are due to the limited set of bias values for which we show data: trajectories do occur with all values of ϕ and k.

Given this strong correlation, we can link the phase transition that takes place at $s = 0$ in this system to the hydrodynamic time scale τ_{LL}, which diverges in the limit of large systems (recall Sec. II A 2). We define the (normalized) autocorrelation function of the system size

$$C_{LL}(t) = \frac{\langle \delta L(t')\delta L(t'+t)\rangle_{eq}}{\langle \delta L(t')^2\rangle_{eq}} \tag{15}$$

which is evaluated at equilibrium (so there is no dependence on t'), with $\delta L = L - \overline{L}$. In the low-pressure limit, this correlation function decays as $e^{-t/\tau_{LL}}$. For the finite pressures considered here, the correlation time is also close to τ_{LL}. Similarly the correlation function of the activity is

$$C_{kk}(t) = \frac{\langle \delta\mathcal{K}(t')\delta\mathcal{K}(t'+t)\rangle_{eq}}{\langle \delta\mathcal{K}(t')^2\rangle_{eq}}, \tag{16}$$

where $\mathcal{K}(t) = \sum_i |r_i(t+\Delta t) - r_i(t) - \Delta\overline{x}(t)|^2$ is the quantity that appears in the definition of the activity K; recall (9). To show the long-time behavior of $C_{kk}(t)$ more clearly we smooth the function by convolving it with a Gaussian window, with variance $\sigma^2 = \tau_B^2/4$: we plot $\Gamma \sum_{t'} C_{kk}(t')e^{-2(t-t')^2/\tau_B^2}$, where the proportionality constant Γ normalizes the correlation function to unity at $t = 0$.

Figure 10 shows that the correlation functions $C_{kk}(t)$ and $C_{LL}(t)$ behave very similarly, consistent with the idea that the activity fluctuations are strongly correlated with those of the global density (and hence to the system size). Since the

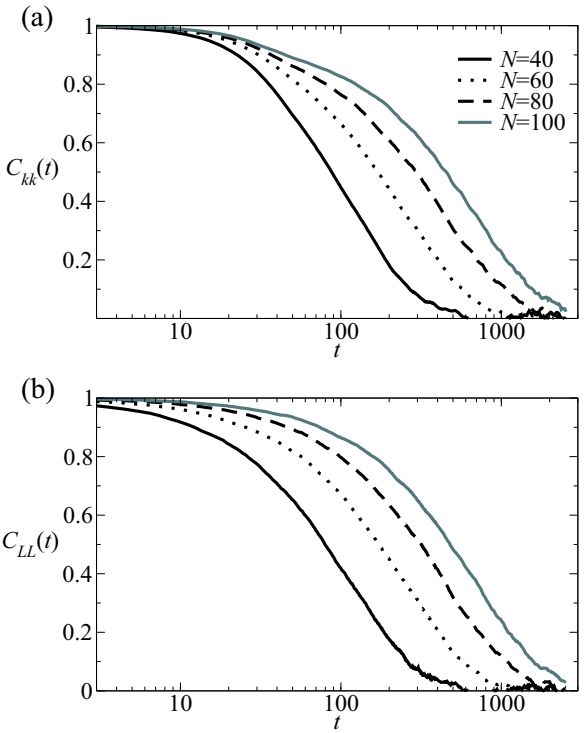

FIG. 10. (Color online) The activity and volume correlation functions for constant pressure systems at equilibrium, for different system sizes. The correlation time τ_{kk} is strongly correlated with τ_{LL}. To display the long-time behavior most clearly, $C_{kk}(t)$ has been smoothed with a Gaussian window (see main text).

volume relaxation time τ_{LL} diverges as $\overline{L}^2$, we therefore expect a similar divergence in the relaxation time of the activity.

This divergent time scale is important because the susceptibility $\chi = -dk/ds$ is related to the autocorrelation function of the activity [30] as

$$\chi(s=0, t_{\rm obs}\to\infty) = \frac{2}{\overline{L}}\int_0^\infty {\rm d}t\, \langle \delta\mathcal{K}(0)\delta\mathcal{K}(t)\rangle_{\rm eq} \qquad (17)$$

so that $\chi \sim \tau_{kk} \sim \overline{L}^2$ diverges at $s=0$, which we interpret as a dynamical phase transition. (The equal time value of the correlator in this equation scales as $\overline{L}$ since $\delta\mathcal{K}$ is extensive in the system size: this $\overline{L}$ dependence cancels with the prefactor so that the right hand side scales with τ_{kk}, with a prefactor of order unity.) Since $\chi = -dk(s)/ds$, the divergence of χ corresponds to a singularity in $k(s)$ and hence a dynamical phase transition. This amounts to a perturbative argument for the existence of the phase transition: a related perturbative argument based on fluctuations at finite wave vector was used in [15] to explain the existence of phase transitions in systems at finite volume.

Recalling the discussion of Sec. III C, the analogous argument for the constant-pressure system is that the noise force η_L in (6) acquires a finite average in the inactive state, resulting in a reduced system size. The previous argument based on τ_{LL} indicates that biasing the noise force in this way requires very little cost in probability: this low cost appears partly because only a single noise term needs to be biased, but also because the absolute size of the bias becomes small in large systems, due to the scaling of the diffusion constant D_L with system size [Eq. (8)].

Finally we note that s^* shifts from a value of order $1/N$ in the constant-density system to a value close to zero at constant pressure. We interpret the small positive s^* (for the constant-volume system) in terms of the probability cost required to form the interface in a phase-separated system at constant density. At constant pressure, no interface is required so the system can have a diverging linear response, as shown in (17).

B. Active state, $s < 0$

In Fig. 11(a), we show the structure factor of the constant-pressure system for $s < 0$. For a given bias s, the fluctuations in the total system size are small in relative terms, so we evaluate the structure factor at wave vectors $q = 2n\pi/L'$ as usual, and calculate $S(q)$ by an ensemble average at fixed n (recall $L' = L - N\ell_0$ is the system size in the representation where particles are treated as pointlike). This provides an estimate of $S(\overline{q})$ with $\overline{q} = 2\pi n/\overline{L'}$. The results of Fig. 11(a) are consistent with hyperuniformity of the active ($s < 0$) phase, although the effect is weaker than that shown in Fig. 6, for the constant-density system. We also show the distribution of particle separations in Fig. 11(b), for comparison with Fig. 5(b). The distribution fits well to an exponential form, independent of s. Given the correlations that are apparent from Fig. 11(a), this result is somewhat surprising: it might be that the correlations are sufficiently weak on short length scales that they are not discernible from $P(d)$.

In this constant-pressure system, it seems that achieving large deviations by changes in structure (for example phase separation or hyperuniformity) is unfavorable compared to changing the system density. Thus, particle separations remain exponentially distributed independent of s, but the system density depends strongly on s. Even at the longest length scales and largest $|s|$ the structure is only weakly affected; compare Figs. 6(a) and 11(a).

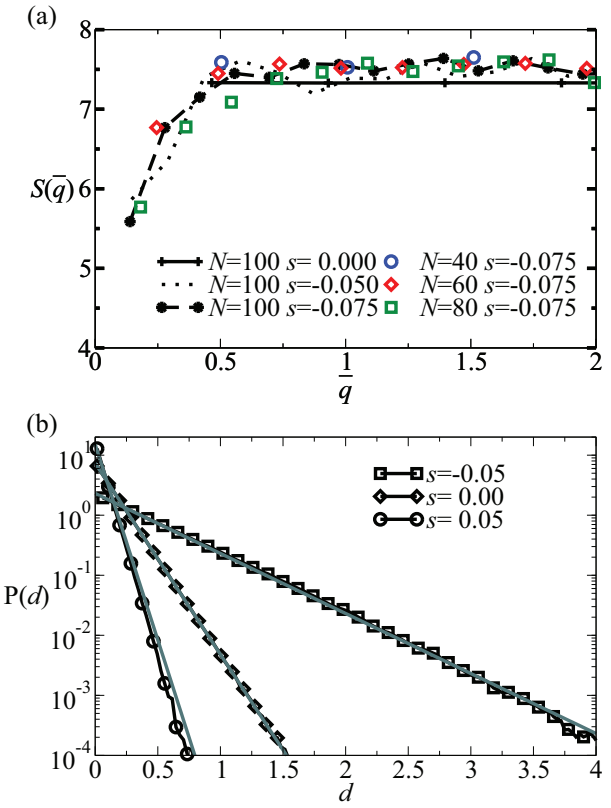

FIG. 11. (Color online) (a) Structure factors in the constant-pressure regime when biased to higher than equilibrium activities. There is a suppression of long-range density fluctuations as in the constant-density active phase. (b) The distribution of separations for a system of $N = 100$ particles. Symbols represent measured distributions, solid lines are exponential distributions with a mean separation calculated from the mean volume. In all regimes the separations are distributed exponentially and are similar to equilibrium, albeit with a different mean separation.

It is possible that a more accurate mimic of the active constant-volume system would be obtained by a constant-pressure system whose pressure was adjusted to match the (fixed) density of the constant-volume one. This would be consistent with the idea that the (virial) pressure in the constant-volume system depends on the bias s. We defer an investigation of this possibility to a future study.

V. DISCUSSION: PRESSURE BALANCE AND MECHANICAL EQUILIBRIUM

In Secs. III and IV, we have presented numerical results for different biases and in different ensembles. To rationalize these results, it is useful to consider the fundamental principles of force balance and mechanical equilibrium in these biased (nonequilibrium) ensembles. Of particular interest is the

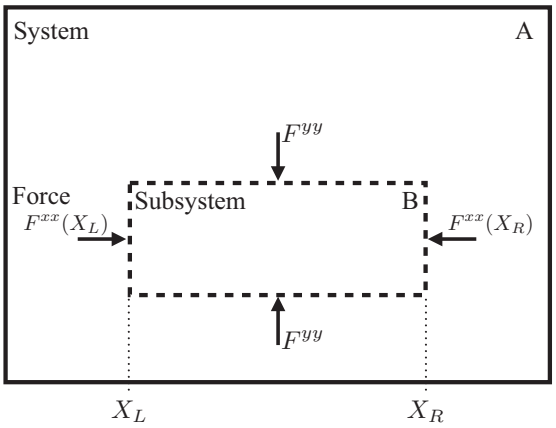

FIG. 12. Schematic illustration of a large system A in which we identify a subsystem B, whose left and right boundaries are at positions X_L and X_R respectively. The particles within the subsystem feel forces from the rest of the system. We assume that the stress is isotropic and homogeneous, so the forces are normal to the subsystem boundaries. The forces are also proportional to the boundary areas: for example $F^{xx} = P^{\rm mech} A_x$ where $P^{\rm mech}$ is the pressure and A_x is the area of the interface (in two dimensions this is simply a length).

phase-separated state shown in Fig. 4(b): this state is stabilized by noise forces in the interfacial region that have nonzero averages (recall Sec. III C). Here we discuss how this can be consistent with a local definition of the pressure, but that this pressure is not equal between the coexisting "phases."

To illustrate the general principles at work, consider the situation shown in Fig. 12, which shows a subsystem B of a large system. The volume of the subsystem is V_B. (Our arguments apply in one spatial dimension and for higher dimensions too: in one dimension V_B is simply the linear size of region B.) As usual in hydrodynamic descriptions, we imagine that the subsystem contains sufficiently many particles that we can define a local pressure, but is small enough that the pressure varies weakly within the subsystem. There are two kinds of forces that act on the subsystem: the conservative interparticle forces coming from particles outside the subsystem, and the noise forces that act on the particles in the subsystem (which may have nonzero averages if $s \neq 0$).

We suppose that the mean conservative forces at the boundaries of the subsystem are everywhere normal to the boundaries, as shown in Fig. 12. (This assumption is trivial in one dimension but in higher dimensions then one could in principle allow for anisotropic local stresses.) The local mechanical pressure $P^{\rm mech} = P^{\rm mech}(x)$ is defined as the force per unit area of boundary, with positive pressure corresponding to forces pointing into the subsystem. (In one dimension, the force per unit area is simply the force at the boundary.) So for example, in Fig. 12, $F^{xx} = P^{\rm mech} A_x$.

The forces acting in this situation are analyzed in Appendix B, under the assumptions that there are no macroscopic particle currents in the steady state of the system, and that the forces at the boundaries come only from the conservative forces between particles. (We neglect any forces from momentum fluxes across the boundaries.) The analysis follows the standard methodology for equilibrium systems [41] (see also [42]). Here we state the main results.

In the steady state, balance of the total forces on the subsystem yields $(\nabla P^{\rm mech})_B = \overline{\mathcal{F}_B}$, where the overbar indicates an average within the (possibly inhomogeneous) steady state, $\mathcal{F}_B = (1/V_B)\sum_{i\,{\rm in}\,B} \xi_i$ is the nonconservative force per unit volume of the subsystem, in which $\xi_i = \eta_i k_{\rm B} T \sqrt{2/D_p}$ is the nonconservative force that corresponds to the random noise η_i, and the sum runs over all particles in the subsystem. The notation $(\nabla P^{\rm mech})_B$ indicates that the pressure gradient is evaluated at the center of subsystem B, under the assumption that ∇P varies weakly over the spatial scale of the (small) subsystem. Since the relation holds for all subsystems, we obtain (Appendix B 1) the general (local) relationship

$$\nabla P^{\rm mech}(x) = \overline{\mathcal{F}(x)}, \tag{18}$$

where $\mathcal{F}(x)$ is the local nonconservative force density. Of course (18) is exactly the relation for an equilibrium system in the presence of both one-body and two-body forces (for example, hydrostatic equilibrium). In equilibrium, the pressure $P^{\rm mech}$ can be calculated from the virial [19,41]. However, in these nonequilibrium (biased) systems, the relation between the mechanical pressure and the virial is different from the equilibrium case. We define a virial for particles in the subsystem as

$$\mathcal{V}_B = \frac{1}{2d} \sum_{ij\,{\rm in}\,B} (x_i - x_j) F_{ij}, \tag{19}$$

where $F_{ij} = \nabla_j v(x_j - x_i)$ is the conservative force on particle i from particle j. Then, as shown in Appendix B 2 the mechanical pressure associated with the subsystem is

$$P^{\rm mech} = \frac{\overline{N_B} k_{\rm B} T + \overline{\mathcal{V}_B} + \overline{\mathcal{P}_B^{\rm act}}}{V_B}, \tag{20}$$

where V_B is the volume of region B, the number of particles in that region is N_B, and

$$\mathcal{P}_B^{\rm act} = \frac{1}{d} \sum_{i\,{\rm in}\,B} \xi_i \delta x_i, \tag{21}$$

where δx_i is the position of particle i, relative to the center of subsystem B. We identify $\overline{\mathcal{P}_B^{\rm act}}/V_B$ as the "swim pressure," as derived in active matter systems [20–23] (in that case the forces ξ_i are the phoretic "swim forces" [43] of the active particles).

There are two important consequences of this analysis. First, to the extent that the swim pressure can be evaluated (as it can in active matter systems and in computer simulations within the s ensemble), Eq. (20) allows a local definition of the pressure, within a biased (or nonequilibrium) system. Second, Eq. (18) shows that this pressure need not be homogeneous: for example, in phase-separated systems such as that shown in Fig. 4, we expect the two dynamical phases to be associated with different values of the local pressure. (The difference in pressure is given by the integral of the one-body force $\mathcal{F}$ across the interface between the phases.) Given this observation, it is not surprising that phase coexistence was not observed in the constant pressure system for $s > 0$: the phases that coexist in the constant-volume system do not have equal pressures. We emphasize that these results are based on several assumptions: we define the pressure in terms of the conservative forces

exerted on a subsystem, and we assume (i) that no macroscopic currents flow in the biased ensemble, and (ii) that the pressure is isotropic everywhere, so that any forces on a subsystem are orthogonal to its boundaries. The possible relationship between these calculations and active-matter systems [20–23] is an interesting direction for future study.

VI. CONCLUSION

We have demonstrated dynamic phase transitions in a one-dimensional model of diffusing particles, including transitions from simple equilibrium fluid states into both high-activity and low-activity states. We considered both constant-density and constant-pressure systems: their transitions share some common features but there are also important differences. Based on the theory of fluctuating hydrodynamics, we argued [15] that the transitions occur for all densities ρ, and the arguments given here indicate that this should also hold for all applied pressures.

Considering first the transition to inactive states, the constant-volume system undergoes phase separation, while the constant-pressure system increases the local density. (As in equilibrium systems, the constant-pressure system avoids interfaces between coexisting phases.) For large systems, the inactive phase occurs for all $s > 0$, in both ensembles. However, there is no signature of phase coexistence in the constant-pressure system: we find only a dense phase, consistent with the different (mechanical) pressures of the coexisting phases in the constant-volume system.

For transitions to high-activity states, the constant-volume system spontaneously suppresses long-range density fluctuations and develops a hyperuniform structure [15]. At constant pressure, the main feature of the high-activity state is that the total density decreases sharply, although there is also some suppression of large-scale density fluctuations.

Overall, these results emphasize that equilibrium ideas of ensemble equivalence do not apply directly when considering large deviation phenomena such as those considered here. While the mechanical pressure and the virial can still be related, the possibility of phase coexistence at unequal pressures shows how familiar equilibrium concepts such as phase separation need to be re-evaluated and generalized in these nonequilibrium settings.

The supporting data for this article are openly available from the University of Bath data archive [44].

ACKNOWLEDGMENTS

We thank P. Sollich and T. Speck for helpful discussions, and the Engineering and Physical Sciences Research Council (EPSRC) for support through Grant No. EP/I003797/1.

APPENDIX A: MONTE CARLO DYNAMICAL SCHEME

1. Constant volume system

The constant-volume system evolves by single particle MC moves [19]. Particle displacements Δx are chosen uniformly from the range $-S \leqslant \Delta x \leqslant S$, with $S = 0.1 l_0$. If the displacement results in a particle overlap, it is rejected; otherwise, it is accepted.

For small time steps and on short time scales (in between collisions), particles undergo diffusive motion: a particles' mean-squared displacement after $N_{\rm MC}$ steps is $N_{\rm MC} S^2/3$. From the Langevin equation (1), we note that the displacement of a particle after a similarly short time t is $2D_p t$. For consistency between Langevin and MC descriptions, we equate these displacements, which shows that the physical time associated with one MC move (per particle) is $t_0 = S^2/(6D_p)$.

When the packing fraction ϕ is large, the rate of acceptance of MC moves can get small, and it becomes convenient to use a rejection-free MC algorithm that operates in continuous time [19,45]. To achieve this, all possible particle displacements are calculated: let g_i denote the fraction of possible moves for particle i that are compatible with the hard-particle interactions (i.e., the fraction that would be accepted). Particle i is selected with probability $g_i/(\sum_j g_j)$ and one of its possible moves is implemented. The simulation time is then incremented by

$$t_i = \frac{\tau_{\rm B}}{N_{\rm MC}} \frac{N}{\sum_j g_j} \ln(1/\mu), \tag{A1}$$

where μ is randomly distributed $0 < \mu \leqslant 1$ [so $\ln(1/\mu)$ is exponentially distributed with a mean of unity]. The process is repeated and moves are made until the total simulation time reaches the desired duration.

2. Constant pressure system

In constant-pressure simulations, the particle coordinates evolve as above. In addition, we also perform MC moves in which we propose changes to the volume of the system. A change in volume is proposed as $L_{\rm new} = L_{\rm old} + \Delta L$ where $-S_L \leqslant \Delta L \leqslant S_L$. The scaled particle positions u_i are the same in the old and new configurations. If the proposed move causes any particles to overlap the move is rejected immediately. Otherwise, the move is accepted with probability $\min(1, e^{-\beta P \Delta L + N \ln(L_{\rm new}/L_{\rm old})})$ [19].

At every MC step, a volume change is proposed with fixed probability $1/N$ and a particle displacement is proposed with probability $(N-1)/N$. The scheme samples the correct equilibrium distribution independent of this probability and independent of the move size S_L. However, to ensure consistency with Eqs. (6) and (8) we specify that the maximum volume change satisfies $S_L^2 = S^2 (2\pi)^2 k_{\rm B} T \kappa_T / \overline{L}$. (Note this depends on the applied pressure, via the mean box size $\overline{L}$.)

APPENDIX B: FORCE BALANCE IN BIASED ENSEMBLES

In this appendix, we consider the forces acting on the subsystem shown in Fig. 12, and we derive a formula for the pressure of this subsystem.

1. Force balance

We first consider force balance. Starting from the equation of motion (1), we sum over all particles inside subsystem B. Taking an average within a (possibly inhomogeneous) steady state and assuming no net currents we have $\overline{\sum_{i \text{ in } B} \dot{x}_i} = 0$. It is convenient to define $\xi_i = \eta_i k_{\rm B} T \sqrt{2/D_p}$, which is the force associated with the noise term η_i in the equation of motion (1).

Hence from (1),

$$\overline{\sum_{i \text{ in } B} \sum_{j \text{ outside } B} F_{ij}} + \overline{\sum_{i \text{ in } B} \xi_i} = 0, \tag{B1}$$

where $F_{ij} = -F_{ji}$ is the conservative (nonstochastic) force exerted on particle i by particle j: in our system $F_{ij} = v'(x_j - x_i)$. Here, $v(x)$ is the interparticle potential [recall (3)] and the prime denotes a derivative. We use an overbar instead of angle brackets to indicate averages within steady states, to avoid possible confusion if ergodicity is broken. For example, if phase separation occurs as in Fig. 4, the steady-state average is taken with a fixed (arbitrary) position of the void, while an ensemble average (indicated here by angle brackets) should include all possible void positions.

The first term (double sum) in (B1) is localized at the boundary of the subsystem. Recalling Fig. 12, we decompose the sum into contributions from the different boundaries. Assuming that the total force on each boundary is normal to that boundary, we take the x component of the forces in (B1). The double sum reduces to $-F^{xx}(X_R) + F^{xx}(X_L)$, since F^{xx} is defined as the sum over the boundary of the forces acting on particles inside the system. Hence (B1) yields

$$-F^{xx}(X_R) + F^{xx}(X_L) + \overline{\mathcal{F}_B^x} = 0, \tag{B2}$$

where $\mathcal{F}_B^x = \sum_{i \text{ in } B} \xi_i^x$ is the x component of the total noise force, We emphasize that the F^{xx} are sums of conservative interparticle forces only.

Recalling $P^{\text{mech}}(X) = F^{xx}(X)/A_x$, where A_x is the area of the boundary, we find

$$\frac{\overline{\mathcal{F}_B^x}}{V_B} = \frac{P^{\text{mech}}(X_R) - P^{\text{mech}}(X_L)}{X_R - X_L}, \tag{B3}$$

where we used $V_B = (X_R - X_L)A_x$. This equation states that any average noise forces on the subsystem must be balanced by conservative forces that act at the subsystem boundaries. We further assume that the pressure drop across the subsystem is small enough to write $P^{\text{mech}}(X_R) - P^{\text{mech}}(X_L) \approx (X_R - X_L)(\partial P^{\text{mech}}/\partial x)$. Considering the other boundaries in a similar way, one arrives at Eq. (18) of the main text.

2. Virial expression for the pressure

We now follow a standard analysis that relates the pressure in a system to the virial [41]. We require a mild generalization in order to include the possibility that noise forces in the Langevin equation have finite averages—a similar situation is considered in [42], for active matter systems. It is useful to refer to Fig. 12. We define the virial for the entire system by

$$\mathcal{V} = \frac{1}{2d} \sum_{ij} (x_i - x_j) F_{ij}, \tag{B4}$$

which includes only the conservative forces.

It is useful to decompose $\mathcal{V}$ into four contributions:

$$\mathcal{V} = \mathcal{V}_B + \mathcal{V}_{AB} + \mathcal{V}_{BA} + \mathcal{V}_A. \tag{B5}$$

Here $\mathcal{V}_B = \frac{1}{2d} \sum_{ij \text{ in } B} (x_i - x_j) F_{ij}$ [recall Eq. (19)] is the contribution from particles entirely inside B, while

$$\mathcal{V}_{AB} = \frac{1}{d} \sum_{i \text{ in } B} \sum_{j \text{ outside } B} x_i F_{ij} \tag{B6}$$

involves particles near the boundary of B. The term $\mathcal{V}_{BA} = \frac{1}{d} \sum_{i \text{ in } B} \sum_{j \text{ outside } B} x_j F_{ji}$ is also localized at the interface, while $\mathcal{V}_A$ involves contributions only from particles outside region B. (We include factors of d in these definitions for later convenience.)

The next step is to relate the mechanical pressure to $\overline{\mathcal{V}_{AB}}$, following [41,42]. We decompose (B6) into a sum over the different boundaries of system B, and decompose each F_{ij} into components parallel and normal to the boundary. For concreteness, consider the rightmost boundary in Fig. 12. All particles at the boundary have $x_i \approx X_R$, so the contribution of this boundary to $\mathcal{V}_{AB}$ is given by $(1/d) \sum_i \sum_j x_i F_{ij} \approx (X_R/d) \sum_i \sum_j F_{ij}^x = -(X_R/d) F^{xx}(X_R)$ where the sums run over particles i that are inside B and close to the relevant boundary, and particles j that are outside B. The second equality comes from the definition of $F^{xx}(X_R)$ as the sum of conservative forces at the boundary. Similarly the leftmost boundary gives a contribution $X_L F^{xx}(X_L)/d$ to $\overline{\mathcal{V}_{AB}}$. The sum of these contributions is

$$\mathcal{V}_{AB}^x = -\frac{1}{2d}(X_R - X_L)[F^{xx}(X_R) + F^{xx}(X_L)] - \frac{1}{2d}(X_R + X_L)[F^{xx}(X_R) - F^{xx}(X_L)], \tag{B7}$$

where the superscript x indicates that we considered only interfaces perpendicular to the x axis. Assuming as before that these quantities vary weakly on the scale of the subsystem, a Taylor expansion of F^{xx} yields

$$\mathcal{V}_{AB}^x \approx -\frac{1}{d}(X_R - X_L)[F^{xx}(X_B) + X_B(\partial F^{xx}/\partial x)] \tag{B8}$$

with $X_B = (X_R + X_L)/2$ the geometrical center of the subsystem. [We have neglected corrections at $O(X_R - X_L)^2$.]

In one spatial dimension, $\mathcal{V}_{AB}$ is given by (B8). In higher dimensions, the virial has other similar contributions that come from the other pairs of parallel interfaces. Incorporating these terms and recalling from Fig. 12 that $P^{\text{mech}} = F^{xx}/A_x$, the generalization of (B8) is

$$\frac{\mathcal{V}_{AB}}{V_B} = -P^{\text{mech}}(X_B) - X_B \cdot \nabla P^{\text{mech}}(X_B), \tag{B9}$$

where we used $A_x(X_R - X_L) = V_B$. Alternatively using (18) we may write

$$\mathcal{V}_{AB} = -P^{\text{mech}}(X_B) V_B - X_B \cdot \overline{\sum_{i \text{ in } B} \xi_i}. \tag{B10}$$

(Recall that $\xi_i = \eta_i k_B T \sqrt{2/D_p}$ is the force corresponding to the stochastic noise η_i.)

The final step is to obtain a formula for the local pressure that depends only on particles inside B. To this end, we use the definitions of the virials to write $\mathcal{V}_B + \mathcal{V}_{AB} = (1/d) \sum_{i \text{ in } B} \sum_j x_i F_{ij} = (1/d) \sum_i x_i F_i$, where $F_i = \sum_j F_{ij}$ is the total conservative force on particle i. From the equation

of motion (1) we have therefore

$$\mathcal{V}_B + \mathcal{V}_{AB} = \frac{1}{d}\sum_{i\text{ in }B} x_i\left(\frac{k_\mathrm{B}T}{D_p}\partial_t x_i - \xi_i\right) = \frac{1}{d}\sum_{i\text{ in }B}\left[\frac{k_\mathrm{B}T}{D_p}\partial_t\left(x_i^2/2\right) - dk_\mathrm{B}T - x_i\xi_i\right], \tag{B11}$$

where we used Ito's formula $\partial_t f(x_t) = f'(x_t)\partial_t x_t + f''(x_t)D_p$.

The analysis at this point is slightly subtle (see also [42]). The simplest approach is to assume that the average of the time derivative $\overline{\partial_t(x_i^2)} = 0$ in the steady state, so we obtain $\overline{\mathcal{V}_B} + \overline{\mathcal{V}_{AB}} = -\overline{N_B}k_\mathrm{B}T - \frac{1}{d}\overline{\sum_{i\text{ in }B} x_i\xi_i}$, where N_B is the number of particles in the subsystem. Using (B10) to substitute for $\mathcal{V}_{AB}$, one finally arrives at

$$P^{\mathrm{mech}}(X_B)V_B = \overline{N_B}k_\mathrm{B}T + \overline{\mathcal{V}_B} + \frac{1}{d}\overline{\sum_{i\text{ in }B}\xi_i(x_i - X_B)} \tag{B12}$$

which is equivalent to (21) of the main text (note $\delta x_i = x_i - X_B$). The terms proportional to $\overline{N_B}$ and $\overline{\mathcal{V}_B}$ are familiar from equilibrium [41] but the final "swim pressure" term is new [23]. Thus Eq. (B11) allows evaluation of the mechanical pressure from knowledge of the positions and noise forces of particles inside subsystem B: see also Eq. (20) of the main text.

Strictly, the assumption that $\overline{\partial_t(x_i^2)} = 0$ can be justified only if particles in B are confined within its boundaries, so that they equilibrate to a constant density profile. For a more precise analysis [42], it is necessary to consider particles that exchange between regions A and B of the system, and the associated momentum fluxes. This case will be analyzed in a future publication.

[1] H. Spohn, J. Phys. A **16**, 4275 (1983).
[2] B. Derrida, J. Stat. Mech. (2007) P07023.
[3] H. Hinrichsen, Adv. Phys. **49**, 815 (2000).
[4] O. Cohen and D. Mukamel, Phys. Rev. Lett. **108**, 060602 (2012).
[5] O. Cohen and D. Mukamel, Phys. Rev. E **90**, 012107 (2014).
[6] H. Touchette, Phys. Rep. **478**, 1 (2009).
[7] V. Lecomte, C. Appert-Rolland, and F. van Wijland, Phys. Rev. Lett. **95**, 010601 (2005).
[8] J. Tailleur and J. Kurchan, Nat. Phys. **3**, 203 (2007).
[9] L. O. Hedges, R. L. Jack, J. P. Garrahan, and D. Chandler, Science **323**, 1309 (2009).
[10] T. Speck and D. Chandler, J. Chem. Phys. **136**, 184509 (2012).
[11] R. Chetrite and H. Touchette, Phys. Rev. Lett. **111**, 120601 (2013).
[12] R. Chetrite and H. Touchette, Ann. Henri Poincare **16**, 2005 (2015).
[13] J. P. Garrahan, R. L. Jack, V. Lecomte, E. Pitard, K. van Duijvendijk, and F. van Wijland, Phys. Rev. Lett. **98**, 195702 (2007).
[14] V. Lecomte, F. van Wijland, and J. P. Garrahan, J. Phys. A: Math. Theor. **45**, 175001 (2012).
[15] R. L. Jack, I. R. Thompson, and P. Sollich, Phys. Rev. Lett. **114**, 060601 (2015).
[16] S. Torquato and F. H. Stillinger, Phys. Rev. E **68**, 041113 (2003).
[17] L. Bertini, A. De Sole, D. Gabrielli, G. Jona-Lasinio, and C. Landim, Rev. Mod. Phys. **87**, 593 (2015).
[18] C. Kipnis and C. Landim, *Scaling Limits of Interacting Particle System* (Springer, Berlin, 1999).
[19] D. Frenkel and B. Smit, *Understanding Molecular Simulation*, 2nd ed. (Academic, San Diego, 2002).
[20] R. Wittkowski, A. Tiribocchi, J. Stenhammar, R. J. Allen, D. Marenduzzo, and M. E. Cates, Nat. Commun. **5**, 4351 (2014).
[21] A. P. Solon, J. Stenhammar, R. Wittkowski, M. Kardar, Y. Kafri, M. E. Cates, and J. Tailleur, Phys. Rev. Lett. **114**, 198301 (2015).
[22] J. Bialke, J. T. Siebert, H. Lowen, and T. Speck, Phys. Rev. Lett. **115**, 098301 (2015).
[23] S. C. Takatori, W. Yan, and J. F. Brady, Phys. Rev. Lett. **113**, 028103 (2014).
[24] N. G. van Kampen, *Stochastic Processes in Physics and Chemistry* (Elsevier, Amsterdam, 2007).
[25] P. L. Krapivsky, K. Mallick, and T. Sadhu, Phys. Rev. Lett. **113**, 078101 (2014).
[26] S. Whitelam, Mol. Simul. **37**, 606 (2011).
[27] C. Appert-Rolland, B. Derrida, V. Lecomte, and F. van Wijland, Phys. Rev. E **78**, 021122 (2008).
[28] T. S. van Erp and P. G. Bolhuis, J. Comput. Phys. **205**, 157 (2005).
[29] P. G. Bolhuis, D. Chandler, C. Dellago, and P. L. Geissler, Annu. Rev. Phys. Chem. **53**, 291 (2002).
[30] J. P. Garrahan, R. L. Jack, V. Lecomte, E. Pitard, K. van Duijvendijk, and F. van Wijland, J. Phys. A **42**, 075007 (2009).
[31] A. A. Budini, Phys. Rev. E **82**, 061106 (2010).
[32] G. L. Eyink, J. Stat. Phys. **61**, 533 (1990).
[33] R. L. Jack, J. P. Garrahan, and D. Chandler, J. Chem. Phys. **125**, 184509 (2006).
[34] T. Bodineau and C. Toninelli, Commun. Math. Phys. **311**, 357 (2012)
[35] M. Plischke and M. Bergersen, *Equilibrium Statistical Physics*, 3rd ed. (World Scientific, Singapore, 2006).
[36] D. Chen, Y. Jiao, and S. Torquato, J. Phys. Chem. B **118**, 7981 (2014).
[37] L. Berthier, P. Chaudhuri, C. Coulais, O. Dauchot, and P. Sollich, Phys. Rev. Lett. **106**, 120601 (2011).
[38] M. Florescu, S. Torquato, and P. J. Steinhardt, Proc. Natl. Acad. Sci. USA **106**, 20658 (2009).
[39] Y. Jiao, T. Lau, H. Hatzikirou, M. Meyer-Hermann, J. C. Corbo, and S. Torquato, Phys. Rev. E **89**, 022721 (2014).
[40] D. Hexner and D. Levine, Phys. Rev. Lett. **114**, 110602 (2015).
[41] J.-P. Hansen and I. R. McDonald, *Theory of Simple Liquids* (Academic, London, 2006).
[42] R. G. Winkler, A. Wysocki, and G. Gompper, Soft Matter **11**, 6680 (2015).
[43] R. Golestanian, T. B. Liverpool, and A. Ajdari, Phys. Rev. Lett. **94**, 220801 (2005).
[44] http://dx.doi.org/10.15125/BATH-00153.
[45] A. B. Bortz, M. H. Kalos, and J. L. Lebowitz, J. Comput. Phys. **17**, 10 (1975).